Behavior of a frustrated quantum spin chain with bond dimerization

Tota Nakamura
Department of Applied Physics, Tohoku University, Sendai, Miyagi 980-77, Japan

Satoshi Takada
Institute of Physics, University of Tsukuba, Tsukuba, Ibaraki 305, Japan

(Received 17 December 1996)

We clarified behavior of the excitation gap in a frustrated $S=1/2$ quantum spin chain with bond dimerization by using the numerical diagonalization of finite systems and a variational approach. The model interpolates between the independent dimer model and the $S=1$ spin chain by changing a strength of the dimerization. The energy gap is minimum at the fully frustrated point, where a localized kink and a freely mobile antikink govern the low-lying excitations. Away from the point, a kink and an antikink form a bound state by an effective triangular potential between them. They finally collapse to a local triplet at a sufficient value of the dimerization. The wave function of the bound state, the consequential gap enhancement, and the localization length of the bound state were obtained exactly in the continuous limit. The gap enhancement obeys a power law with exponent 2/3. We also obtained the dispersion relation of the local triplet excitation for the entire phase space. The method and the obtained results are common to other frustrated double spin-chain systems, such as the one-dimensional J_1-J_2 model, or the frustrated ladder model. [S0163-1829(97)03021-X]

I. INTRODUCTION

Recently, the interest in the field of the low-dimensional quantum systems is concentrated on systems with a spin gap, especially in connection with the high-T_c cuprates upon doping.[1] The ground state of such a system realizes the spin disordered singlet state, favored by a quantum fluctuation and/or frustration. The excitation energy gap opens above the ground state. As typical models, we can consider the spin ladder model,[2–4] the bond-alternation model,[3] and the Majumdar-Ghosh model.[5,6]

Syntheses of various new compounds[7] also accelerate investigations on this field both theoretically and experimentally. For example, magnetic susceptibility measurement on $KCuCl_3$ (Ref. 8) indicates a spin gap behavior, and the experimental data are considered to be explained theoretically by the double spin-chain model with frustration.[9] Estimation of the magnitude of the gap through the susceptibility data is already established on the assumption of the dimer gap.[10] However, it is not sufficient to the thorough understanding of the system. We must investigate the origin of the gap and the physical picture of the excited states. This is a main purpose of this paper.

The Δ chain, the subject model in the present paper, is a participant of double spin-chain systems, but has rather special geometry of the interaction bonds. The triangles are aligned in one direction. If we connect the spins located at the top of the triangles with the interaction bonds, it becomes the railroad-trestle model. Therefore, it may seem that the interesting properties are peculiar to this special system.

The early investigations on the Δ chain were directed in search for a system with the singlet dimer ground state.[11–14] They were restricted to a symmetric case where all the interaction bonds are set equal, and thus the system is fully frustrated. In this case, the ground state is the singlet dimer state with twofold degeneracy under the periodic boundary conditions. Interpretation of the excited states by a kink and an antikink was done at this stage.[11,12] The existence of the finite energy gap above the ground state was rigorously proven.[14] Analogy of the model to the kagomé antiferromagnet has been pointed out:[15] there are macroscopic local continuous degeneracy in the ground state in the classical limit, low-lying excitation spectrum is consequently dispersionless, and there exists an additional peak of the specific heat at low temperatures. The origin of the dispersionless mode and the double peak of the specific heat were recently clarified.[16,17] Sen *et al.*[17] also pointed out that the possible relevance of the model to the newly synthesized compound, $YCuO_{2.5}$.

In this paper, we find that the Δ chain possesses common features with other spin gap systems besides its unique properties stated above. Concretely, we mean the ''common feature'' by the way the system reduces frustration by the bond dimerization, which results in an asymmetric Δ chain. This is an essence of this paper.

The ground state in a fully frustrated system is generally unstable against a small perturbation that relaxes strong frustration. It must have a strong influence on the low-lying excited states as well, and consequently to the low-temperature behavior of various physical quantities. We should take this effect into account when we analyze the experimental data. We consider the bond dimerization as a perturbation, since its energy stabilization is the strongest one, and it can be realized by a lattice distortion as in the spin-Peierls systems.[18]

From a theoretical point of view, the frustrated double spin-chain systems with the bond dimerization are very attractive. They have the dimer state and the $S=1$ Haldane state in both extremes of the strength of the dimerization parameter. In the midst is the fully frustrated point. As was shown in the F-AF bond-alternation model,[3] there always exist the string order of den Nijs and Rommelse[19] and the dimer order.[20] The dimer state continuously changes to the

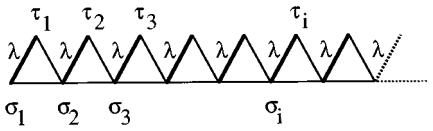

FIG. 1. Shape of the dimerized Δ chain. Bold lines indicate the λ bonds.

$S=1$ Haldane state with the increase of strength of the ferromagnetic interaction bonds.[21,22] Therefore, there is always a finite energy gap. Then questions arise. How do we identify these two phases? How do the differences manifest in the observable physical quantities? In this paper, we show by adopting the Δ chain for an example that the whole phase space can be divided into three regions with respect to the nature of the first excited state relevant to the energy gap, and that the differences affect the low-temperature dependences of physical observables such as the specific heat and the susceptibility.

Section II describes the model and summarizes the general remarks concerning the symmetric Δ chain without the dimerization, which will be the starting point of the discussion in Sec. III. In the first part of Sec. III, we do the same variational analysis as was done in the symmetric Δ chain.[16,17] This is valid only for positively (antiferromagnetically) small dimerization. Then, continuous limit of the effective Hamiltonian is derived and its exact solution is obtained. The remaining part of Sec. III is devoted to the case when the dimerization is negatively (ferromagnetically) small. We use the nonlocal unitary transformation[21–24] to represent the ground state and the excited state. This transformation is equivalent to the Kennedy-Tasaki transformation of the $S=1$ system, and is its adaptation to the double spin-chain systems. The transformation is powerful when the ground state is either in the Haldane state or in the state with strong dimer correlation. Almost equivalent results to the positive dimerization case are obtained near the symmetric point. We show how the system converges to the Haldane state and the dimer state in Sec. IV. Section V shows the differences of the observable quantities between two phases. We also propose a quantity to judge the phase in experiments. Section VI is devoted to summary and discussion.

II. THE MODEL AND GENERAL REMARKS

We consider a system described by the following Hamiltonian:

$$\mathcal{H}=\sum_{n=1}^{N} \lambda \boldsymbol{\sigma}_n\cdot\boldsymbol{\tau}_n+\boldsymbol{\tau}_n\cdot\boldsymbol{\sigma}_{n+1}+\boldsymbol{\sigma}_n\cdot\boldsymbol{\sigma}_{n+1}. \tag{1}$$

Here, N is the number of the triangles in the system, λ is a parameter denoting the dimerization, and $|\boldsymbol{\sigma}|=|\boldsymbol{\tau}|=1/2$. Figure 1 shows the depicted lattice. At the point $\lambda=1$, the system is the symmetric Δ chain and is fully frustrated. In the limit of $\lambda=+\infty$, the system reduces to the independent dimer model. In the other limit of $\lambda=-\infty$, the system becomes equivalent to the $S=1$ spin chain. Therefore, the present model has the independent dimer ground state and the Haldane ground state in its extremes.

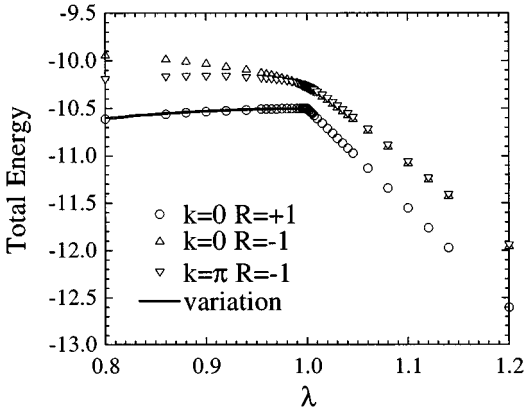

FIG. 2. The λ dependence of the energy of the lowest state in the subspace denoted by k (wave number), and R (spin reversal symmetry) in the system with $N=14$ (28 spins). We also plot the variational estimate for the ground state energy for $\lambda<1$ (solid line).

The understandings of the symmetric Δ chain are already established.[16,17] Here, we briefly summarize the results. The ground state is the perfect singlet dimer state with twofolded degeneracy in the case of the periodic boundary conditions. The low-lying excited states approximately consist of $(N-1)$ singlet dimers and two free spins. The excitations are governed by sets of two free spins named a ''kink'' and an ''antikink.'' A kink stays localized and works as a delimiter to moving antikinks. Dispersionless aspects of the excitations originate in a localized kink. An antikink is considered as a free particle moving between kinks with the effective mass. An antikink is supposed to be one free spin only within the first approximation, since it is not an eigenstate of the local Hamiltonian. It spreads out to an extent in reality. A detailed structure of an antikink is not revealed yet, but it merely renormalizes the effective mass. Within the first approximation, the mass $m=1$. The second approximation that an antikink is distributed among five spin sites gives the mass $m=1.158$,[17] and the numerical diagonalization data after the $N\rightarrow\infty$ extrapolation shows the mass $m=1.21$.[16] The excitation gap is well expressed by a summation of a kinetic energy of an antikink and the creation energy of a pair of a kink and an antikink, $\epsilon_0=0.215$, as

$$\Delta E=\epsilon_0+\frac{1}{m}\left(1-\cos\frac{\pi k}{N}\right), \tag{2}$$

where k is the wave number of an antikink alone. The low-temperature peak of the specific heat can be reproduced by the Schottky specific heat with the gap expressed above.[16] Susceptibility was also calculated.[17]

III. IN THE VICINITY OF $\lambda=1$

We numerically diagonalized the above Hamiltonian up to the systems with 28 spins ($N=14$) under the periodic boundary conditions. The λ dependence of the energy is shown in Fig. 2. The ground state energy is highest at the fully frustrated point ($\lambda=1$), which leads to the instability due to the lattice dimerization.

For $\lambda>1$, the ground state is always the pure dimer state which consists of the singlet dimers on every λ bond. Thus the total ground state energy is exactly $-0.75\lambda N$. We refer to this state as the left-dimer state hereafter in this paper. In this region, the spin correlation length vanishes. The excited states also have no k dependence. At $\lambda=1$, the ground states are twofold degenerate under the periodic boundary conditions. They are the left-dimer state and the right-dimer state. The first-order transition occurs at this point. For $\lambda<1$, the correlation length gradually increases with decreasing λ. The right-dimer state smoothly reaches the $S=1$ Haldane state in the limit of $\lambda=-\infty$ without any phase transition. Hereafter, we simply call the region $\lambda>1$ as the dimer phase, and the region $\lambda<1$ as the Haldane phase. The degeneracy of the excited states in the dimer phase is lifted in the Haldane and a state with $k=\pi$ becomes the first excitation.

A. λ>1: The dimer phase

The results obtained in this subsection have already been reported briefly.[25] We discuss the method and the results in detail in this paper.

The excited states in this phase may have similar properties to those at the symmetric point, because the ground state is the same. Therefore, we do the same variational analysis as was successful at $\lambda=1$.[16,17] The boundary conditions are set open, though they do not influence the final results in the thermodynamic limit. We define a variational basis ψ_i so that an antikink is located at the ith triangle

$$\psi_i \equiv \psi_{\rm kink}\otimes[4,5]\cdots[2i-2,2i-1]\uparrow_{2i} \times[2i+1,2i+2]\cdots[2N-1,2N], \tag{3}$$

where $[i,j]$ denotes a singlet dimer state connecting the ith and the jth site, namely $[i,j]=(\uparrow_i\downarrow_j-\downarrow_i\uparrow_j)/\sqrt{2}$ for $\uparrow_i(\downarrow_i)$ denoting an up (down) spin located at the ith site. Here, we numbered the site so that $\boldsymbol{\sigma}_n$ is the $(2n-1)$th, and $\boldsymbol{\tau}_n$ is the $(2n)$th as is shown in Fig. 1. The $\uparrow_{2i}$ above is an antikink. The wave function of a kink located at the leftmost edge is known as

$$\psi_{\rm kink}=[\uparrow_1(\uparrow_2\downarrow_3-\downarrow_2\uparrow_3)+\uparrow_2(\uparrow_1\downarrow_3-\downarrow_1\uparrow_3)]/\sqrt{6}. \tag{4}$$

This state is an eigenstate of the edge triangle Hamiltonian, and therefore does not move. Its energy eigenvalue is $\lambda/4-1$. Thus a kink contributes to the excitation energy by $(\lambda-1)$. The singlet dimers, $\{[2n,2n+1]\}$, existing between a kink and an antikink are not eigenstates of local triangle Hamiltonians. They also contribute to the excitation energy.

The variational basis is not orthogonal to each other and satisfies the following relations:

$$\langle\psi_i|\psi_j\rangle=\left(\frac{1}{2}\right)^{|i-j|}, \tag{5}$$

$$\langle\psi_i|\mathcal{H}|\psi_j\rangle=\left[E_{\rm g}+(\lambda-1)+\frac{3}{4}(\lambda-1)\min(i,j)\right]\langle\psi_i|\psi_j\rangle + \frac{3}{4}\delta_{ij}. \tag{6}$$

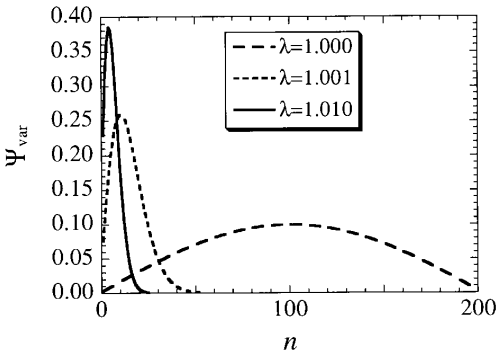

FIG. 3. Variational wave function of an antikink in the lowest excited state for $\lambda=1.00, 1.001$, and 1.01. Size of the system $N=200$. n stands for the location of an antikink.

Here, δ_{ij} is the Kronecker delta, and $\min(i,j)=i$ if $i\leqslant j$. Our task is to find a function $\Psi_{\rm var}\equiv\Sigma_i C_i\psi_i$ that minimizes the energy expectation,

$$\mathrm{Var}E\equiv\frac{\langle\Psi_{\rm var}|\mathcal{H}|\Psi_{\rm var}\rangle}{\langle\Psi_{\rm var}|\Psi_{\rm var}\rangle}=\frac{\Sigma_{i,j}C_iC_j\langle\psi_i|\mathcal{H}|\psi_j\rangle}{\Sigma_{i,j}C_iC_j\langle\psi_i|\psi_j\rangle}. \tag{7}$$

If we diagonalize the denominator and rewrite the numerator with its eigenfunction, this variational problem is transformed into a simple eigenvalue problem. Then, the solution of Eq. (7) can be obtained by the numerical diagonalization for a finite system size. We show the result of $N=200$ in Fig. 3 with $\lambda=1.00$, 1.001, and 1.01. In the case of the symmetric Δ chain ($\lambda=1.00$), the wave function is the sine function indicating a free motion of an antikink. An antikink is drastically attracted to a kink as λ increases. The wave function exhibits an antikink localized. We clarify the wave function analytically by using the continuous limit.

We rewrite the above equation by the new basis $|\phi_k\rangle=\Sigma_n\exp[ikn]|\psi_n\rangle$, since the denominator of Eq. (7) is diagonalized by Fourier transformation in the large N limit. Note that k is the wave number of an antikink alone, and does not correspond to the total wave number. Then the basis relations become

$$\langle\phi_k|\phi_l\rangle=\frac{3}{5-4\cos k}\delta_{k,l}+\frac{4\cos\dfrac{l-k}{2}-5\cos\dfrac{l+k}{2}}{\left(2\cos l-\dfrac{5}{2}\right)\left(2\cos k-\dfrac{5}{2}\right)} \times\frac{1-2^{-N}}{N}, \tag{8}$$

$$\langle\phi_k|\mathcal{H}|\phi_l\rangle=[E_{\rm g}+(\lambda-1)]\langle\phi_k|\phi_l\rangle+\frac{3}{4}\delta_{k,l}+\frac{3}{4}(\lambda-1)A_{k,l}, \tag{9}$$

with

$$A_{k,l}=\frac{1}{N}\sum_{n,m}\exp[i(kn-lm)]\min(m,n)\langle\psi_n|\psi_m\rangle. \tag{10}$$

The diagonal elements of $A_{k,l}$ dominate the off-diagonal elements. Then, $A_{k,k}$ is written as

$$A_{k,k}=\frac{1}{N}\frac{6-13\cos k+8\cos 2k}{\frac{245}{4}-87\cos k+30\cos 2k+4\cos 3k}$$
$$+\frac{4-5\cos k}{\frac{33}{4}-10\cos k+2\cos 2k}+\frac{N+1}{2}\frac{3}{5-4\cos k}. \tag{11}$$

We find in this equation that $A_{k,k}$ diverges in the limit $N\to\infty$. In order to avoid this divergence, we introduce a cutoff factor $i\delta$ to the momentum, namely $k\to k+i\delta/2$. This should have no effect on physical results by taking the limit $\delta\to 0$ after $N\to\infty$. We rewrite the matrix element and pick up only the leading term of the off-diagonal part and the terms up to the k^2 in the diagonal part. Then the continuous limit, $N\to\infty$ and $k\to 0$, of the Hamiltonian $\tilde{\mathcal{H}}_{k,l}$ is given by

$$\tilde{\mathcal{H}}_{k,l}\doteq\left(E_{\mathrm{g}}+(\lambda-1)+\frac{1}{4}+\frac{k^2}{2}\right)\delta_{k,l}$$
$$+\frac{1}{N}\frac{3}{4}(\lambda-1)\frac{1}{(k-l+i\delta)^2}. \tag{12}$$

Apart from the constant terms, this Hamiltonian is equivalent to the following in the real space representation:

$$\mathcal{H}_C=-\frac{1}{2m}\frac{d^2}{dx^2}+\frac{3}{4}(\lambda-1)x\exp[-\delta x]. \tag{13}$$

Here, x is the distance between a kink and an antikink; m is the effective mass of an antikink and is set $m=1$ in the first approximation. We take the limit $\delta\to 0$ at this stage. The first term is the kinetic energy of an antikink, and the second term is the triangular potential attracted by a localized kink. We rescale x by $X=\theta x$ with $\theta=(3m(\lambda-1)/2)^{-1/3}$. Then the eigenvalue equation $\mathcal{H}_C\Psi=E_C\Psi$ becomes

$$\left(-\frac{d^2}{dX^2}+X\right)\Psi=E'\Psi, \tag{14}$$

where $E'=E_C\times 2m\theta^2$. Its solution is known as the Airy function, $\Psi=A_i(X-E')$ with the first eigenvalue $E'\simeq(3\pi/2\times 0.7587)^{2/3}\simeq 2.338$.[26] Accordingly, we can obtain the energy eigenvalue E_C, the average distance between a kink and an antikink $\langle x\rangle$, and the localization length of the wave function ξ,

$$E_C=\frac{E'}{2m\theta^2}=1.532m^{-1/3}(\lambda-1)^{2/3}, \tag{15}$$

$$\langle x\rangle=\frac{2}{3}E'\theta=1.362m^{-1/3}(\lambda-1)^{-1/3}, \tag{16}$$

$$\xi\sim 5\times\theta=4.368m^{-1/3}(\lambda-1)^{-1/3}. \tag{17}$$

The localization length, ξ, is obtained from a rough estimation of the localization length of the Airy function ~ 5. The estimation of ξ is quite consistent with the wave function shown in Fig. 3: $\xi\sim 40$ for $\lambda=1.001$, and $\xi\sim 20$ for $\lambda=1.01$. It should be noticed that $\frac{3}{4}(\lambda-1)A_{k,k}/\langle\phi_k|\phi_k\rangle$ of Eqs. (8) and (9) becomes equivalent to E_C, if we replace N by ξ above.

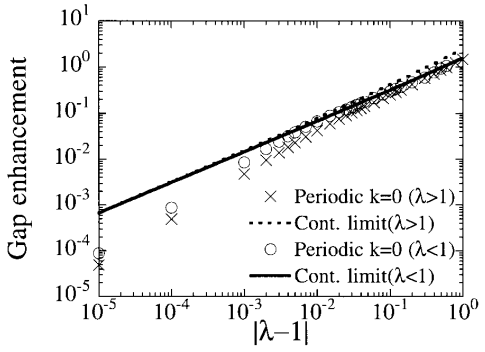

FIG. 4. Log-log plot of the gap enhancement for the exact result in the continuous limit with the mass $m=1.21$, and the numerical results of the periodic system with $N=14$.

Now, the total gap behavior can be obtained from the kink contribution, $(\lambda-1)$, and the antikink contribution, E_C. The gap enhancement defined by $\Delta_{\mathrm{Gap}}=E_{\mathrm{gap}}(\lambda)-E_{\mathrm{gap}}(1)$ is

$$\Delta_{\mathrm{Gap}}=(\lambda-1)+1.5319\times m^{-1/3}(\lambda-1)^{2/3}. \tag{18}$$

The gap increases in a power law with its exponent 2/3. As a consequence, the gap rapidly increases with λ, and is doubled at $\lambda=1.06$. Figure 4 shows the behavior of the gap enhancement, Δ_{Gap}, compared with the numerical results of the periodic system of $N=14$. We used a value of the mass, $m=1.21$, estimated at $\lambda=1$ (Ref. 16) for better comparison. For $\lambda-1>0.01$, the numerical data agree with the analytical estimation. In this region, the localization length is within the finite system size, $\xi<14$.

The relevant excitation in this region is governed by a competition between the kinetic energy and the triangular potential energy of an antikink. When the dimerization is small, an antikink gains energy by the kinetic motion. As the dimerization becomes large, an antikink is bound by a kink, and finally they collapse to a local triplet. The exponent 2/3 is a general outcome of this competition.

B. λ<1: The Haldane phase

In this region, the ground state cannot be known trivially, although we can expect the right-dimer state continuously changes to the $S=1$ Haldane state in the limit of $\lambda\to-\infty$.[20–22] We make use of the nonlocal unitary (NLU) transformation for the double spin-chain systems,[21–24] the second-order perturbation, and the numerical diagonalization to clarify the ground state first. Then we proceed to investigate the excited state by using the variational method and the numerical diagonalization. We clarify how the physical pictures of the lowest excitation changes with λ. Recently, Brehmer *et al.* have investigated the phase diagram and the hidden order for generalized spin-ladder models.[4] They have used the matrix product states for the variational calculation of the ground state, which was shown to be equivalent to our present variational method.[4,27]

We transform the Hamiltonian $\mathcal{H}$ with U defined in Appendix A. We obtain

$$U^{-1}\mathcal{H}U=\sum_{n=1}^{N}\lambda\boldsymbol{\sigma}_n\cdot\boldsymbol{\tau}_n-(\sigma_n^x+\tau_n^x)\tau_{n+1}^x-(\sigma_n^z+\tau_n^z)\sigma_{n+1}^z$$
$$-4(\sigma_n^z\tau_n^x+\sigma_n^x\tau_n^z)\sigma_{n+1}^z\tau_{n+1}^x, \quad (19)$$

from Eq. (A8) in the Appendix. According to this transformation, string order parameters are transformed into local parameters such as $\langle\sigma_n^x\rangle$, $\langle\sigma_n^z\rangle$, $\langle\sigma_n^z\tau_n^x\rangle$, as will be found in Eqs. (31) and (32). It makes possible that we employ a single-site approximation like the molecular-field one. Thus we consider the following variational trial function for the ground state:

$$|\Psi_0\rangle=\prod_{n=1}^{N}|n(b)\rangle=\prod_{n=1}^{N}(b|T_n\rangle+\sqrt{1-b^2}|S_n\rangle), \quad (20)$$

$$|S_n\rangle=(|\uparrow,\downarrow\rangle-|\downarrow,\uparrow\rangle)/\sqrt{2}, \quad (21)$$

$$|T_n\rangle=\alpha|\uparrow,\uparrow\rangle+\beta(|\uparrow,\downarrow\rangle+|\downarrow,\uparrow\rangle)/\sqrt{2}+\gamma|\downarrow,\downarrow\rangle. \quad (22)$$

$|\uparrow,\uparrow\rangle$'s are the state of $|\sigma_n^z,\tau_n^z\rangle$. b,α,β,γ are the variational parameter and satisfy the normalization condition, $\alpha^2+\beta^2+\gamma^2=1$. These parameters are supposed to be invariant of n. The analysis is variational in this sense. A state with $b=0$ is the left-dimer state on the λ bonds, a state with $b=\sqrt{3}/2$ is the right-dimer state, and a state with $b=1$ corresponds to the pure valence bond solid (VBS) state in this representation. The energy expectation value is calculated as

$$\langle\Psi_0|\mathcal{H}|\Psi_0\rangle=\left[\lambda\left(b^2-\frac{3}{4}\right)-b^4\left(\frac{(\alpha^2-\gamma^2)^2}{2}+2\beta^2(\alpha^2+\gamma^2)\right)\right.$$
$$\left.-3b^3\sqrt{1-b^2}\beta(\alpha^2-\gamma^2)\right]N. \quad (23)$$

We can easily find this minimum value and the variational parameter set by using the Lagrange multiplier. The energy value ϵ_0 is

$$\lambda\left(b^2-\frac{3}{4}\right)-\frac{2}{3}b^4-\frac{2b^3\sqrt{3(1-b^2)}}{3}\equiv\epsilon_0, \quad (24)$$

with four possible choices of the parameters (α,β,γ) as

$$(\alpha,\beta,\gamma)=(\pm\sqrt{2/3},\sqrt{1/3},0),(0,-\sqrt{1/3},\pm\sqrt{2/3}), \quad (25)$$

and b determined through

$$\lambda=\frac{4}{3}b^2-\frac{b(4b^2-3)}{\sqrt{3(1-b^2)}}, \quad (26)$$

or

$$b=0. \quad (27)$$

The fourfold degeneracy in the choice of α,β,γ corresponds to the degeneracy of the edge states.[21,24,28] A state with $b=0$ is the singlet dimer ground state for $\lambda>1$. The other one, Eq. (26), corresponds to the ground state for $\lambda<1$. If we solve Eq. (26) up to the second order of $(1-\lambda)$,

$$b=\frac{\sqrt{3}}{2}\left[1+\frac{1-\lambda}{4}-\frac{5}{16}(1-\lambda)^2\right]. \quad (28)$$

Then the energy expectation per triangle is

$$E/N=-\frac{3}{4}-\frac{3}{16}(1-\lambda)^2. \quad (29)$$

This agrees with the result due to the second-order perturbation of $(\lambda-1)\boldsymbol{\sigma}_n\cdot\boldsymbol{\tau}_n$. Details of the calculation are given in Appendix B. The diagonalization result of a finite system with 14 triangles shown in Fig. 2 is fitted by the least-square method to

$$E/N=-\frac{3}{4}-\frac{3.0176}{16}(1-\lambda)^2-0.003(1-\lambda). \quad (30)$$

Consistency between the analytic estimation and the numerical result is excellent as is shown in Fig. 2.

We can also estimate the string order parameter of den Nijs and Rommelse, $O_{\rm str}$,[19] and the dimer order parameter, $O_{\rm dim}$.[20,21] The definitions and the expectation values are

$$O_{\rm dim}=\lim_{|m-n|\to\infty}-4\left\langle U^{-1}\tau_m^z\exp\left[i\pi\sum_{k=m+1}^{n-1}S_k^z\right]\sigma_n^zU\right\rangle$$
$$=\lim_{|m-n|\to\infty}4\langle\sigma_m^z\sigma_n^z\rangle=4\langle\sigma_m^z\rangle\langle\sigma_n^z\rangle=4\langle\sigma_m^z\rangle^2$$
$$=\frac{4}{9}b^4+\frac{4}{3}b^2(1-b^2)+\frac{8}{9}b^3\sqrt{3(1-b^2)}, \quad (31)$$

$$O_{\rm str}=\lim_{|m-n|\to\infty}-\left\langle U^{-1}S_m^z\exp\left[i\pi\sum_{k=m+1}^{n-1}S_k^z\right]S_n^zU\right\rangle$$
$$=\lim_{|m-n|\to\infty}\langle S_m^zS_n^z\rangle=\langle S_m^z\rangle\langle S_n^z\rangle=\langle S_m^z\rangle^2=\frac{4}{9}b^4. \quad (32)$$

At $\lambda=1$, $O_{\rm dim}=1$ as $b=\sqrt{3}/2$. In the limit of $\lambda\to-\infty$, it converges to the VBS value $O_{\rm dim}=4/9$ as $b\to1$. On the other hand, the string order parameter, $O_{\rm str}$ takes a value of $O_{\rm str}=1/4$ at $\lambda=1$ and converges to the same value of $O_{\rm dim}=O_{\rm str}=4/9$. It should be noted that the convergence of $b\to1$ is very fast that it takes a value $b=0.94$ even at $\lambda=0.25$. Therefore, the Haldane state can be realized even if all the interaction bonds are antiferromagnetic.

Figure 5 shows the dimer and the string order parameter of the ground state in the whole phase space. Numerical data are of the periodic system with $N=12$. Quantitative agreement is excellent near $\lambda=1$. The string order increases as λ decreases from 1. Therefore, we call the region $\lambda<1$ the Haldane phase. It should be noted that the numerical data converge to the value of $S=1$ ($\simeq0.37$) (Ref. 29) in the limit of $\lambda\to-\infty$, not to the value of the pure VBS state. The contradiction becomes distinct at $\lambda\sim-1$, where the string order parameter takes the maximum value. This is because we used the variation of the single-site approximation as in Eq. (20), besides the correlation length is rather large in the Haldane state.

A low-energy excitation is intrinsically of domain-wall type in one dimension. Two perfect singlet dimer states, $|n(\sqrt{3}/2)\rangle$ and $|n(0)\rangle$, are degenerate at $\lambda=1$. For $\lambda<1$, the latter state becomes the excited state and the former state

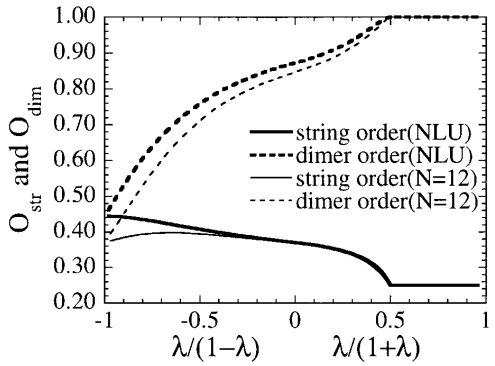

FIG. 5. The string order parameter and the dimer order parameter are plotted against $\lambda/(1-\lambda)$ for $\lambda<0$, and against $\lambda/(1+\lambda)$ for $\lambda>0$. Bold lines are the analytic estimate obtained by the nonlocal unitary transformation. Thin lines are numerical diagonalization results of the lattice with 12 triangles.

becomes the ground state by changing the value of b. Therefore, we consider the following wave function as a trial for the excited state:

$$|\Psi_1\rangle=\sum_i C_i\psi_i=\sum_i C_i\left(\prod_{n=1}^{i}|n(b)\rangle\prod_{n=i+1}^{N}|n(0)\rangle\right). \quad (33)$$

Because the state $|n(0)\rangle$ becomes a higher excited state for $\lambda<1$, the validity of this trial wave function is restricted to the very vicinity of $\lambda=1$. The domain wall located at the ith triangle is essentially an antikink before the NLU transformation is done. Thus the analysis is for a kink-antikink excitation. The basis relations of ψ_i are

$$\langle\psi_i|\psi_j\rangle=(\sqrt{1-b^2})^{|i-j|}, \quad (34)$$

$$\langle\psi_i|\mathcal{H}_l|\psi_j\rangle=[E_g+E_1(N-\min(i,j))+E_2\delta_{i,j}]\langle\psi_i|\psi_j\rangle, \quad (35)$$

with $E_g=\epsilon_0 N$, $E_1=-0.75\lambda-\epsilon_0$, and $E_2=\lambda(b^2-0.75)-\epsilon_0$. These relations are equivalent to the ones in the previous subsection, Eqs. (5) and (6). Therefore, the problems are solved in the same way and we obtain

$$E_C=1.856m^{-1/3}E_1^{2/3}, \quad (36)$$

$$\langle x\rangle=1.237m^{-1/3}E_1^{-1/3}, \quad (37)$$

$$\xi\sim 3.969m^{-1/3}E_1^{-1/3}, \quad (38)$$

for the excitation of $k=0$. However, we remark that the lowest excitation is the state with $k=\pi$ in this region. This state is considered as that both a kink and an antikink are mobile with the total momentum π. The analysis on the state of $k=\pi$ will be done in the next subsection. Three estimates, Eqs. (36), (37), and (38) above, however, have quite good consistency with the second excited state with $k=0$.

IV. AWAY FROM λ=1

Away from the fully frustrated point, $\lambda=1$, the excitation is no longer of a kink-antikink type. They already collapse to a local triplet state. Therefore, we must consider another type of a domain wall for a trial wave function.

In the region of $\lambda<1$, the ground state has fourfold degeneracy associated with the edge states. Within the scheme of our variational analysis, it appears in the four possible choices of the variational parameter (α,β,γ) of Eq. (25). The most natural candidate for the domain wall is the one between any two of the fourfold degenerate ground states. In fact, Fáth and Sólyom[28] showed that the lowest excitation in the AKLT model[30] is of this type. The trial wave function we consider is then

$$|\Psi_1\rangle=\sum_i C_i\psi_i=\sum_i C_i\left(\prod_{n=1}^{i}|n(b)\rangle\prod_{n=i+1}^{N}|n'(b)\rangle\right), \quad (39)$$

where $|n(b)\rangle$ and $|n'(b)\rangle$ only differ the choice of the set (α,β,γ). We use the set $(\alpha,\beta,\gamma)=(\sqrt{2/3},\sqrt{1/3},0)$ for $|n(b)\rangle$, and $(\alpha,\beta,\gamma)=(-\sqrt{2/3},\sqrt{1/3},0)$ for $|n'(b)\rangle$. b is common and determined by Eq. (26). The basis relations are calculated in the same way as

$$\langle\psi_i|\psi_j\rangle=\left(1-\frac{4}{3}b^2\right)^{|i-j|}\equiv(-a)^{|i-j|}, \quad (40)$$

$$\langle\psi_i|\mathcal{H}|\psi_j\rangle=[E_g+(|i-j|-1)E_1+\delta_{i,j}(E_1+E_2)]\langle\psi_i|\psi_j\rangle, \quad (41)$$

with

$$E_1=-\frac{2}{3}b^3\left(b+\sqrt{3(1-b^2)}+\frac{3a}{(b+\sqrt{3(1-b^2)})^3}\right), \quad (42)$$

$$E_2=\frac{8}{9}b^3(b+\sqrt{3(1-b^2)}). \quad (43)$$

In the thermodynamic limit, the above matrices are diagonalized by the Fourier transformation. An expectation value of the energy gap above the ground state is estimated as

$$\begin{aligned}E_{\rm ex}(k)&=\frac{\langle\phi_k|\mathcal{H}|\phi_k\rangle}{\langle\phi_k|\phi_k\rangle}-E_g\\&=-E_1\left(1+\frac{2a}{1-a^2}\frac{(1+a^2)\cos k+2a}{1+2a\cos k+a^2}\right.\\&\quad\left.-\frac{1+2a\cos k+a^2}{1-a^2}\right)+E_2\frac{1+2a\cos k+a^2}{1-a^2}. \quad (44)\end{aligned}$$

$E_{\rm ex}(k)$ always takes minimum at $k=\pi$. The energy gap $E_{\rm ex}(\pi)$ converges to 1/9 in the VBS limit, $\lambda\to-\infty$.

We can also discuss excited states of $\lambda>1$ with this variational scheme, since the domain wall of Eq. (39) can express the local triplet domain wall, if we change the notation of the pair, $\boldsymbol{\sigma}_n$ and $\boldsymbol{\tau}_n$. Unless, the variational solution for the ground state only gives the state with $b=0$, since the exact ground state is the left-dimer state on λ bonds. Then, the variation with $b=0$ gives nothing at all. It should be noticed that a basic recipe of the present variational method is that a spin pair, $\boldsymbol{S}_n=\boldsymbol{\sigma}_n+\boldsymbol{\tau}_n$, should be chosen so that it does not take a singlet dimer state. Therefore, we shift $\boldsymbol{\sigma}$ spins by one site as $\boldsymbol{\sigma}_n\to\boldsymbol{\sigma}_{n+1}$. With this new definition of $\boldsymbol{\sigma}_n$ and $\boldsymbol{\tau}_n$, the left-dimer ground state is represented by $b=\sqrt{3}/2$, or in other words, $a=0$. Expressions of E_1 and E_2 become differ-

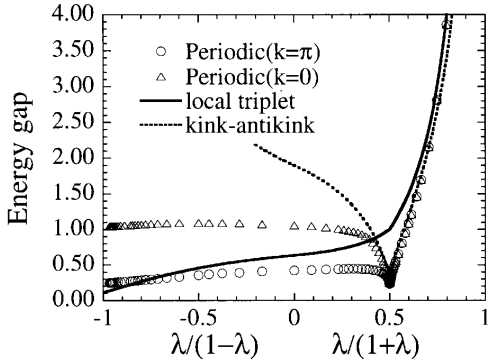

FIG. 6. λ dependence of the energy gap obtained by the numerical diagonalization (circles), the variation of a kink-antikink type (broken line), and the variation of a local triplet type (solid line). The second excitation gap with $k=0$ (triangles) is also plotted. x axis is $\lambda/(1-\lambda)$ for $\lambda<0$, and $\lambda/(1+\lambda)$ for $\lambda>0$.

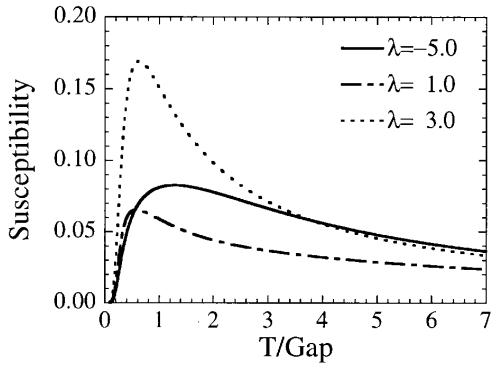

FIG. 7. Uniform susceptibility per spin calculated for $\lambda=-5.0, 1.0$, and 3.0 by the exact diagonalization of the finite systems with the periodic boundary conditions. The size of the system is $N=7$. Each λ represents the Haldane phase, the fully frustrated point, and the dimer phase, respectively.

ent from Eqs. (42) and (43), and are $E_1=-\lambda/2-1/4$ and $E_2=\lambda$, respectively. The excitation is calculated dispersionless as

$$E_{\mathrm{ex}}(k)=\lambda. \tag{45}$$

This result is nothing but the local triplet excitation, where one singlet dimer is replaced by a triplet in the ground state. This becomes the exact solution in the limit $\lambda\to\infty$.

Figure 6 shows the λ dependence of the energy gap obtained by the variation and the numerical diagonalization of the periodic system with 24 spins. The numerical results are depicted by symbols. The variational results of a kink-antikink type excitation, Eqs. (15) and (36), are shown by a broken line; those of a local triplet excitation, Eqs. (44) and (45), are shown by a solid line. We also plot the second excitation gap for the comparison with Eq. (36).

In the dimer phase, $\lambda>1$, consistency between the numerical and the variation is excellent. Estimations by the kink-antikink variation are better in the vicinity of $\lambda=1$, while those of the local triplet become better as λ increases. This crossover occurs at $\lambda\sim3$, where the average distance between a kink and an antikink $\langle x\rangle$ of Eq. (16) becomes unity. On the other hand, the consistency in the region, $\lambda<1$, only remains in a qualitative level. Within the single-site approximation employed in this paper, $\boldsymbol{\sigma}$ spins and $\boldsymbol{\tau}$ spins are equivalent to each other. For example, $\langle n(b)|\boldsymbol{\sigma}_n\cdot\boldsymbol{\sigma}_{n+1}|n(b)\rangle$ is equal to $\langle n(b)|\boldsymbol{\tau}_n\cdot\boldsymbol{\tau}_{n+1}|n(b)\rangle$. Therefore, the approximation should be better for the system with a symmetry of exchanging $\boldsymbol{\sigma}\leftrightarrow\boldsymbol{\tau}$. Since the present model does not possess this symmetry, the estimation is not good. It should be excellent in the symmetric systems such as the Majumdar-Ghosh model.[31] We must go beyond the single-site approximation to improve the estimates in the Haldane phase of the Δ chain. The numerical data converge to the value, ~0.24 consistent with the $S=1$ system; half the gap of a typical diagonalization result of $S=1$ system with 12 spins, 0.4842.[32] Only the number of interaction bonds between $\boldsymbol{S}_n$ and $\boldsymbol{S}_{n+1}$ determines the strength of the effective interaction, since $\boldsymbol{\sigma}_n$ and $\boldsymbol{\tau}_n$ become symmetric in the $S=1$ limit. The present model has only two interaction bonds, which corresponds to half the effective interaction in the $S=1$ system.

V. OBSERVABLES

We calculated the magnetic susceptibility and the specific heat of finite system ($N=7$) with periodic boundary conditions in order to see the difference of observable physical quantities between the dimer phase and the Haldane phase. In other words, we try to determine the phase by these observables. Figure 7 shows the uniform magnetic susceptibility for $\lambda=-5.0, 1.00$, and 3.0. These parameters correspond to the Haldane phase, fully frustrated point, and the dimer phase, respectively. We rescale the temperature by each energy gap in order to see the qualitative differences, namely $E\to(E-E_{\mathrm{g}})/E_{\mathrm{gap}}$. The peak width and the height among three are quite different. Data of the dimer phase have a sharp peak, while they become broad in the Haldane phase. This reflects the structure and the density of the excited states, i.e., many continuum states of multiple-magnon excitations in the Haldane phase bring about a broad peak. Contrary, the degeneracy in the excited states in the dimer phase is considered to be smaller compared with the Haldane phase, which generates a rather narrow peak. Full width at half maximum (FWHM) of the peak for each data in the unit of T/Gap is ~2 for $\lambda=3.0$, ~4 for $\lambda=1.0$, and ~6 for $\lambda=-5.0$. The FWHM is almost three times as wide in the Haldane phase as in the dimer phase. We speculate that this value might be a judge to determine the phase. Recently, we have also calculated the susceptibility of the frustrated ladder model, and the J_1-J_2 model with bond dimerization (J_1-J_2-J_3 model), and found that the FWHM take almost the same value as the present case. Details are reported elsewhere.[31]

Figure 8 shows the specific heat. Qualitative tendency is the same as the susceptibility, except for the data of $\lambda=1.00$ showing the double peak structure, which is characteristic of the kink-antikink excitation.[16] Data of the dimer phase are explained by the Schottky type specific heat.

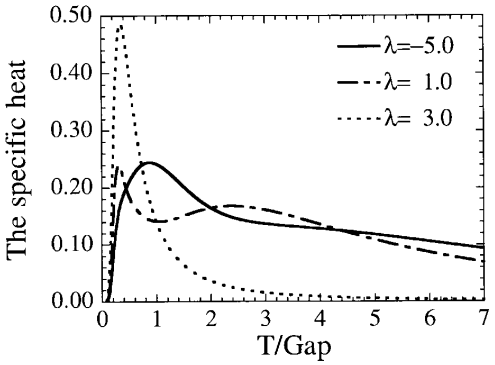

FIG. 8. The specific heat per spin calculated for $\lambda=-5.0, 1.0,$ and 3.0 by the exact diagonalization of the finite systems with the periodic boundary conditions. The size of the system is $N=7$.

VI. SUMMARY AND DISCUSSION

We have investigated the Δ chain with the bond dimerization. The model interpolates the independent dimer model and the $S=1$ spin chain model by changing λ. As for the ground state, the first order transition between the dimer phase and the Haldane phase occurs at $\lambda=1$. To be strict, the ground state for $\lambda>1$ is the perfect singlet dimer state, while that for $\lambda<1$ continuously changes from the dimer state at $\lambda=1$ to the $S=1$ Haldane state at $\lambda=-\infty$.

As for the excited state, we can distinguish the intermediate region, in the vicinity of $\lambda=1$, from the dimer region and the Haldane region. This region is characterized by strong frustration. The energy gap is very small caused by the unstable ground state. The ground state has strong dimer correlation. The excited state is governed by two free spin called a kink and an antikink. They become a local triplet in the dimer and the Haldane region. We can conclude that the intermediate region serves as a buffer between the other two regions.

We clarified the wave function of the bound state of a kink and an antikink, and how they collapse to a local triplet. The essential point is that a kink and an antikink is bound by the triangular potential and the competition between this attractive potential and the kinetic energy causes the gap enhancement with exponent 2/3. The triangular potential is an outcome of unfavored singlet dimers between a kink and an antikink. This mechanism generally occurs when the frustration is relaxed by bond dimerization. For example, Chitra *et al.* investigated the one-dimensional J_1-J_2 model with the bond alternation and found that the gap behaves with $\delta^{2/3}$ with the alternation parameter δ.[33] This might be explained in the same manner as in the present model.

We have also calculated the uniform susceptibility and the specific heat to see how the phases are characterized by the physical observables. We clarified the qualitative difference between the Haldane phase and the dimer phase. The susceptibility data show a broad peak in the Haldane phase, accompanied by continuum multiple magnon excitations. Therefore the FWHM of the peak may serve to judge which phase the data belong to.

ACKNOWLEDGMENTS

The authors would like to thank Professor K. Kubo and Professor A. Oshiyama for valuable discussions. They also acknowledge thanks to Professor H. Nishimori for his diagonalization package, Titpack Ver. 2. Computations were performed partly on Facom VPP500 at the ISSP, University of Tokyo.

APPENDIX A: NONLOCAL UNITARY TRANSFORMATION

In this appendix, we summarize the nonlocal unitary transformation for the double $S=1/2$ spin-chain systems. The transformation is defined by U in the following:

$$U=\prod_{n=1}^{N} U_n, \tag{A1}$$

$$U_n=P_n^{+}+P_n^{-}\exp[i\pi S_n^x], \tag{A2}$$

$$P_n^{\pm}=\frac{1}{2}\left(1\pm\exp\left[i\pi\sum_{k=1}^{n-1}S_k^z\right]\right), \tag{A3}$$

$$\boldsymbol{S}_n=\boldsymbol{\sigma}_n+\boldsymbol{\tau}_n, \tag{A4}$$

where P_n^{+} (P_n^{-}) is the projection operator onto states with the even (odd) number of $S_i^z=\pm 1$ for $i\leqslant n-1$. The spin operators, σ_n^x, σ_n^y, σ_n^z, are transformed as

$$U\sigma_n^x U=\exp\left[i\pi\sum_{m=n+1}^{N}S_m^x\right]\sigma_n^x, \tag{A5}$$

$$U\sigma_n^y U=\exp\left[i\pi\sum_{k=1}^{n-1}S_k^z\right]\exp\left[i\pi\sum_{m=n+1}^{N}S_m^x\right]\sigma_n^y, \tag{A6}$$

$$U\sigma_n^z U=\exp\left[i\pi\sum_{k=1}^{n-1}S_k^z\right]\sigma_n^z. \tag{A7}$$

In the above derivation, the following relations are utilized:

$$U^{-1}=U,\quad U_nU_m=U_mU_n,$$

$$(\exp[i\pi S^{\alpha}])^2=1,\quad \sigma_n^x P_n^{\pm}=P_n^{\mp}\sigma_n^x,$$

$$\sigma_n^{\alpha}\exp[i\pi S_n^{\beta}]=-\exp[i\pi S_n^{\beta}]\sigma_n^{\alpha}\quad(\alpha\neq\beta),$$

$$\exp[i\pi S_n^{\alpha}]\exp[i\pi S_n^{\beta}]\exp[i\pi S_n^{\gamma}]=1(\text{for cyclic }\alpha,\beta,\gamma),$$

which are easily obtained by using $\exp[i\pi\sigma_n^{\alpha}]=2i\sigma_n^{\alpha}$. Transformations for $\boldsymbol{\tau}_n$ are obtained by replacing σ by τ. By using the above relations, exchange interactions become

$$U\boldsymbol{\sigma}_n\cdot\boldsymbol{\tau}_nU=\boldsymbol{\sigma}_n\cdot\boldsymbol{\tau}_n,$$

$$U\boldsymbol{\sigma}_n\cdot\boldsymbol{\sigma}_{n+1}U=-\sigma_n^x\tau_{n+1}^x-\tau_n^z\sigma_{n+1}^z-4\sigma_n^x\tau_{n+1}^x\tau_n^z\sigma_{n+1}^z, \tag{A8}$$

$$U\boldsymbol{\tau}_n\cdot\boldsymbol{\sigma}_{n+1}U=-\tau_n^x\tau_{n+1}^x-\sigma_n^z\sigma_{n+1}^z-4\tau_n^x\tau_{n+1}^x\sigma_n^z\sigma_{n+1}^z.$$

APPENDIX B: SECOND-ORDER PERTURBATION OF THE GROUND STATE ENERGY FOR $\lambda<1$

In this appendix, we show that the second-order perturbation of the ground state energy can be done in this case

without knowing an excited state. We divide the Hamiltonian $\mathcal{H}$ into the unperturbed part $\mathcal{H}_0$ and the perturbation part $\mathcal{H}_1$: $\mathcal{H}=\mathcal{H}_0+\mathcal{H}_1$, where

$$\mathcal{H}_0=\sum_{n=1}^{N} \boldsymbol{\sigma}_n\cdot\boldsymbol{\tau}_n+\boldsymbol{\sigma}_n\cdot\boldsymbol{\sigma}_{n+1}+\boldsymbol{\tau}_n\cdot\boldsymbol{\sigma}_{n+1}, \tag{B1}$$

$$\mathcal{H}_1=(\lambda-1)\sum_{n=1}^{N-1} \boldsymbol{\tau}_n\cdot\boldsymbol{\sigma}_{n+1}. \tag{B2}$$

Here, note that the location of $\boldsymbol{\sigma}_n$ and $\boldsymbol{\tau}_n$ is different from Eq. (19) and Fig. 1 so that the pair $\boldsymbol{S}_n=\boldsymbol{\sigma}_n+\boldsymbol{\tau}_n$ takes the singlet dimer state for the unperturbed Hamiltonian. The unperturbed ground state $|\psi_0\rangle$ is a direct product of singlet dimer states $|S_n\rangle$ on the spin pair $\boldsymbol{\sigma}_n$ and $\boldsymbol{\tau}_n$, i.e.,

$$|\psi^0\rangle=\prod_{n=1}^{N}|S_n\rangle. \tag{B3}$$

Let us first examine the first order perturbation E_1:

$$E_1=\langle\psi^0|\mathcal{H}_1|\psi^0\rangle=(\lambda-1)\sum_{n=1}^{N-1}\langle\psi^0|\psi_n^1\rangle, \tag{B4}$$

where

$$|\psi_n^1\rangle=\boldsymbol{\tau}_n\cdot\boldsymbol{\sigma}_{n+1}|\psi^0\rangle=-\frac{\sqrt{3}}{4}\prod_{k\neq n,n+1}^{N}|S_k\rangle|T_n^2\rangle. \tag{B5}$$

$|T_n^2\rangle$ denotes a singlet state formed by two triplet pairs of $\boldsymbol{S}_n$ and $\boldsymbol{S}_{n+1}$, i.e.,

$$|T_n^2\rangle=(|0_n\rangle|0_{n+1}\rangle-|1_n\rangle|(-1)_{n+1}\rangle-|(-1)_n\rangle|1_{n+1}\rangle)/\sqrt{3}. \tag{B6}$$

$|0_n\rangle,|1_n\rangle$, and $|(-1)_n\rangle$ denote triplet states of a pair $\boldsymbol{S}_n=\boldsymbol{\sigma}_n+\boldsymbol{\tau}_n$ with their eigenvalues of $S_n^z=\sigma_n^z+\tau_n^z$.

It follows from Eqs. (B4) and (B5) that

$$E_1=0, \tag{B7}$$

since the singlet state $|S_n\rangle$ is orthogonal to the triplet state. It is found in Eq. (B5) that the operation $\boldsymbol{\tau}_n\cdot\boldsymbol{\sigma}_{n+1}$ on $|\psi^0\rangle$ transforms the two singlets $|S_n\rangle$ and $|S_{n+1}\rangle$ into triplets leaving the other singlets unchanged.

The second-order perturbation E_2 is calculated as

$$\begin{aligned}E_2&=-\left\langle\psi^0\middle|\mathcal{H}_1\frac{1}{\mathcal{H}_0-E_0}\mathcal{H}_1\middle|\psi^0\right\rangle\\&=-(\lambda-1)^2\sum_{n,m=1}^{N-1}\left\langle\psi_m^1\middle|\frac{1}{\mathcal{H}_0-E_0}\middle|\psi_n^1\right\rangle\\&=\frac{(\lambda-1)^2}{E_0}\sum_{n,m=1}^{N-1}\sum_{k=0}^{\infty}\left\langle\psi_m^1\middle|\left(\frac{\mathcal{H}_0}{E_0}\right)^k\middle|\psi_n^1\right\rangle.\end{aligned} \tag{B8}$$

To proceed further, we divide $\mathcal{H}_0$ into a diagonal part and an off-diagonal part when it operates to $|\psi_n^1\rangle$. An off-diagonal part $\mathcal{H}_n^{\mathrm{OD}}$ is

$$\mathcal{H}_n^{\mathrm{OD}}=(\boldsymbol{\sigma}_{n+1}+\boldsymbol{\tau}_{n+1})\cdot\boldsymbol{\sigma}_{n+2}. \tag{B9}$$

A diagonal part is the rest of the Hamiltonian, $\mathcal{H}_0-\mathcal{H}_n^{\mathrm{OD}}$. The eigenvalue of this diagonal part is $E_1^D=E_0+1=-3N/4+1$. On the other hand, the operation of $\mathcal{H}_n^{\mathrm{OD}}$ to $|\psi_1\rangle_n$ generates a state with three triplets located at the nth, the $(n+1)$th, and the $(n+2)$th triangles, and these triplets form a singlet state. Namely,

$$|\psi_n^2\rangle=\mathcal{H}_n^{\mathrm{OD}}|\psi_n^1\rangle=\frac{1}{\sqrt{2}}\prod_{k\neq n,n+1,n+2}|S_k\rangle|T_n^3\rangle, \tag{B10}$$

where the three-triplets state

$$\begin{aligned}|T_n^3\rangle=\frac{1}{\sqrt{6}}[&(|1_{n+2}\rangle|(-1)_{n+1}\rangle-|(-1)_{n+2}\rangle|1_{n+1}\rangle)\\&\times|0_n\rangle+(|1_{n+1}\rangle|(-1)_n\rangle-|(-1)_{n+1}\rangle|1_n\rangle)|0_{n+2}\rangle\\&+(|1_n\rangle|(-1)_{n+2}\rangle-|(-1)_n\rangle|1_{n+2}\rangle)\times|0_{n+1}\rangle]\end{aligned} \tag{B11}$$

forms a singlet state. Now we get

$$\mathcal{H}_0|\psi_n^1\rangle=E_1^D|\psi_n^1\rangle+|\psi_n^2\rangle. \tag{B12}$$

Similarly, we find

$$\mathcal{H}_0|\psi_n^2\rangle=E_2^D|\psi_n^2\rangle+|\psi_n^3\rangle, \tag{B13}$$

where E_2^D denotes diagonal energy and the $|\psi_n^3\rangle$ is a new state with four triplets forming a singlet state located at the triangle site from n to $n+3$. In general, we have

$$(\mathcal{H}_0)^k|\psi_n^1\rangle=(E_1^D)^k|\psi_n^1\rangle+\sum_{l=2}^{k+1}C_l|\psi_n^l\rangle, \tag{B14}$$

where $|\psi_n^l\rangle$ contains $l+1$ triplets at triangle sites $n,\ldots,n+l$ forming a singlet state; and C_l is a constant. Thus we obtain

$$\begin{aligned}\langle\psi_m^1|\mathcal{H}_0^k|\psi_n^1\rangle&=\delta_{n,m}(E_1^D)^k\langle\psi_m^1|\psi_n^1\rangle\\&=\delta_{n,m}(E_1^D)^k\frac{3}{16}.\end{aligned} \tag{B15}$$

Finally, we get the energy correction of the second order

$$\begin{aligned}E_2&=\frac{3}{16}\frac{(\lambda-1)^2}{E_0}\sum_{n=1}^{N-1}\sum_{k=0}^{\infty}\left(\frac{E_1^D}{E_0}\right)^k\\&=-\frac{3}{16}(\lambda-1)^2(N-1)\frac{1}{E_1^D-E_0}\\&=-\frac{3}{16}(\lambda-1)^2(N-1).\end{aligned} \tag{B16}$$

This agrees with the variational result given by Eq. (29) in the text.

[1] For example, E. Dagotto and T. M. Rice, Science **271**, 618 (1996).
[2] T. Narushima, T. Nakamura, and S. Takada, J. Phys. Soc. Jpn. **64**, 4322 (1995); K. Hida, *ibid*. **64**, 4896 (1995); Y. Nishiyama, N. Hatano, and M. Suzuki, *ibid*. **64**, 1967 (1995), and references therein.
[3] K. Hida, in *Computational Physics as a New Frontier in Condensed Matter Research*, edited by H. Takayama *et al.* (The Physical Society of Japan, Tokyo, 1995), p. 187, and references therein.
[4] S. Brehmer, H-J. Mikeska, and U. Neugebauer, J. Phys. Condens. Matter **8**, 7161 (1996).
[5] C. K. Majumdar and D. Ghosh, J. Math. Phys. **10**, 1388 (1969).
[6] B. S. Shastry and B. Sutherland, Phys. Rev. Lett. **47**, 964 (1981).
[7] A. P. Ramirez, Annu. Rev. Mater. Sci. **24**, 453 (1994).
[8] H. Tanaka, K. Takatsu, W. Shiramura, and T. Ono, J. Phys. Soc. Jpn. **65**, 1945 (1996).
[9] T. Nakamura and K. Okamoto (unpublished).
[10] M. Troyer, H. Tsunetsugu, and D. Würtz, Phys. Rev. B **50**, 13 515 (1994).
[11] M. W. Long and R. Fehrenbacher, J. Phys. Condens. Matter **2**, 2787 (1990).
[12] M. W. Long and S. Siak, J. Phys. Condens. Matter **2**, 10 321 (1990).
[13] F. Monti and A. Sütö, Phys. Lett. A **156**, 197 (1991).
[14] F. Monti and A. Sütö, Helv. Phys. Acta **65**, 560 (1992).
[15] K. Kubo, Phys. Rev. B **48**, 10 552 (1993).
[16] T. Nakamura and K. Kubo, Phys. Rev. B **53**, 6393 (1996).
[17] D. Sen, B. S. Shastry, R. E. Walstedt, and R. Cava, Phys. Rev. B **53**, 6401 (1996).
[18] K. Okamoto, H. Nishimori, and Y. Taguchi, J. Phys. Soc. Jpn. **55**, 1458 (1986), and references therein; for a review, L. V. Interrante, I. S. Jacobs, and J. C. Bonner, in *Extended Linear Chain Compounds*, edited by J. S. Miller (Plenum Press, New York, 1983), Vol. 3, p. 353.
[19] M. den Nijs and K. Rommelse, Phys. Rev. B **40**, 4709 (1989).
[20] K. Hida, Phys. Rev. B **45**, 2207 (1992).
[21] S. Takada, J. Phys. Soc. Jpn. **61**, 428 (1992).
[22] K. Hida and S. Takada, J. Phys. Soc. Jpn. **61**, 1879 (1992).
[23] T. Kennedy and H. Tasaki, Phys. Rev. B **45**, 304 (1992).
[24] S. Takada and K. Kubo, J. Phys. Soc. Jpn. **60**, 4026 (1991).
[25] T. Nakamura and S. Takada, Phys. Lett. A **225**, 315 (1997).
[26] F. Stern, Phys. Rev. B **5**, 4891 (1972).
[27] S. Takada and H. Watanabe, J. Phys. Soc. Jpn. **61**, 39 (1992).
[28] G. Fáth and J. Sólyom, J. Phys. Condens. Matter **5**, 8983 (1993).
[29] S. R. White and D. A. Huse, Phys. Rev. B **48**, 3844 (1993).
[30] I. Affleck, T. Kennedy, E. Lieb, and H. Tasaki, Phys. Rev. Lett. **59**, 799 (1987); Commun. Math. Phys. **115**, 477 (1988).
[31] T. Nakamura, S. Takada, K. Okamoto, and N. Kurosawa (unpublished).
[32] T. Sakai and M. Takahashi, Phys. Rev. B **42**, 1090 (1990).
[33] R. Chitra, S. Pati, H. R. Krishnamurthy, D. Sen, and S. Ramasesha, Phys. Rev. B **52**, 6581 (1995).